remote sensing

MDPI

Article

Evaluation of CFOSAT Wave Height Data with In Situ Observations in the South China Sea

Bo Li [1,2], Junmin Li [1,2,*], Shilin Tang [1], Ping Shi [1], Wuyang Chen [1] and Junliang Liu [1]

[1] State Key Laboratory of Tropical Oceanography, Key Laboratory of Science and Technology on Operational Oceanography, South China Sea Institute of Oceanology, Chinese Academy of Sciences, Guangzhou 511458, China
[2] Sanya Institute of Ocean Eco-Environmental Engineering, Sanya 572025, China
* Correspondence: jli@scsio.ac.cn

Abstract: The wave spectrometer operated by the China–France Oceanography Satellite (CFOSAT) can provide global ocean wave observation data. Although a lot of work on calibration and verification has been carried out in the open oceans dominated by swells, the quality of the data in the relatively enclosed sea area with complex terrain still lacks sufficient examination. The objective of this study is to assess the performance of the significant wave height data of the CFOSAT in the South China Sea (SCS), a unique sea area characterized by semi-enclosed basin and multi-reef terrain, and to recognize the environmental factors affecting the data quality. Compared against the long-term observations from five mooring or buoy sites, we find that the data is well performed in the relatively open and deep areas of the SCS, with an average correlation coefficient as high as 0.87, and a low average root-mean-square error of 0.47 m. However, the combined effects of complex topography, monsoons, and swell proportion variation will affect the performance of data. In the southern deep areas, the waves may be affected by a large number of dotted reefs, leading to wave deformations and energy dissipation in different seasons. In the northern nearshore areas, waves tend to be sheltered by the land or distorted by the shallow topography effects. These processes make it difficult for the swell to fully develop as in the open oceans. The low proportion of swell is a disadvantage for the CFOSAT to correctly observe the wave data and may lead to possible errors. Our results emphasize the importance of more verification when applying the CFOSAT data in certain local seas, and the necessity to adjust the algorithm of inverting wave spectra according to specific environmental factors.

Keywords: CFOSAT; significant wave height; in situ observation; the South China Sea

check for updates

Citation: Li, B.; Li, J.; Tang, S.; Shi, P.; Chen, W.; Liu, J. Evaluation of CFOSAT Wave Height Data with In Situ Observations in the South China Sea. *Remote Sens.* **2023**, *15*, 898. https://doi.org/10.3390/rs15040898

Academic Editors: Jian Sun, Weizeng Shao, Changlong Guan and Alexander Babanin

Received: 3 January 2023
Revised: 22 January 2023
Accepted: 3 February 2023
Published: 6 February 2023

Copyright: © 2023 by the authors. Licensee MDPI, Basel, Switzerland. This article is an open access article distributed under the terms and conditions of the Creative Commons Attribution (CC BY) license (https://creativecommons.org/licenses/by/4.0/).

1. Introduction

The Surface Waves Investigation and Monitoring (SWIM) instrument onboard the China–France Oceanography Satellite (CFOSAT) can provide wave spectra using its off-nadir beams. The instrument obtains the sea surface mirror and quasi-mirror scattering information at different incident angles by transmitting one nadir beam (0°) and five low incidence beams (2°, 4°, 6°, 8°, and 10°) with rotating scanning. Based on the modulation information of the wave tilt on the scattering coefficient in multi-azimuths, the directional wave spectrum and the wave parameters such as significant wave height (SWH) can be obtained based on the spectrum [1–3].

The products of SWIM spectra in its early version of data were quite noisy. Therefore, many authors have made great efforts to improve the quality of wave data [3–8]. For example, Wang et al. [5] developed a method for retrieving the SWH over an extended swath based on the synchronous observations of SWIM and the scatterometer onboard CFOSAT, and achieved significantly increased spatial coverage and promising accuracy. Jiang et al. [6] present a merged mean wave period retrieval model combining the nadir wind speed, SWH, and the mean wave period from the off-nadir spectrum using a simple artificial neural network. Thanks to the joint efforts of these authors, the quality of CFOSAT data has been greatly improved.

Most of the in situ observations used to evaluate or calibrate the CFOSAT data are based on National Buoy Data Center (NBDC) buoys on global scales, especially on the east and west coasts of North America, e.g., [4,6,9]. In those oceans, the path of wave propagation is very open and swells are usually well-developed and account for a large proportion [10,11]. In contrast, for marginal seas, such as the South China Sea (SCS), which is located at the edge of the Western Pacific Ocean, there are still few analyses and studies on the CFOSAT data quality, probably due to the shortage of in situ observation data.

The SCS has complex geographical and climatical environmental features. For example, the SCS is dominated by the monsoons and the wave propagation direction changes seasonally [12,13]. At the same time, the swell energy is introduced from the Luzon Strait to the northeast and spread to the southwest [14]. However, due to the relative closure of the sea basin and the complexity of underwater topography caused by numerous islands and reefs, swell propagation is restricted and energy dissipation is significant [15–17]. In addition, when traversing nearshore areas, waves will be shielded by the land and will deform with shoaling, refraction, and diffraction processes [13,18,19]. As a result, the occurrence probability and wave energy ratios of the SCS swells are significantly lower than those of the global open oceans, including the North Pacific and North Atlantic where the wave data from CFOSAT has been adequately verified.

Due to the relatively low swell energy proportion in the SCS, the performance of the CFOSAT wave data may not be as good as that from open oceans. For example, previous studies have shown that there may be obvious errors in the wavelength data derived from the initial products of CFOSAT under certain sea conditions in the local regions of the southern SCS [7]. By comparing the data of southern deep regions and northern coasts of the SCS, it is further found that the bias of data in shallow water areas is significantly higher than that in deep waters, and it is necessary to eliminate the data with large errors for shallow water area [20]. Therefore, it is still necessary to carry out a more systematic analysis of the impact of typical environmental characteristics of the SCS, such as swell proportion, complex topography, and seasonal variations, on the general performance of the CFOSAT wave data.

For this reason, this study systematically evaluated the quality of the latest version of CFOSAT wave data in the SCS using five sets of in situ observation data, which span nearly three years (November 2018 to October 2022). Based on the data, the impact of nearshore factors such as land shelter and shallow topography, changes in swell components, and their seasonality on the data quality are discussed.

2. Data and Methods

This study assesses two kinds of SWIM data: nadir SWH (SWHn) and spectrometer SWH (SWHs) by off-nadir wave spectrum. In situ SWH from moorings and buoys are used as reference data for SWIM SWH appraisal. In addition, ERA5 data are used to help separate the wind sea and swell. They also provide a seasonal wind pattern in SWH evaluation.

2.1. CFOSAT Wave Data

The latest version of the CFOSAT product is adopted to extract the data in the SCS. The CFOSAT was launched in China in October 2018 to survey the length, height, and direction of waves with the SWIM sensor designed and developed by France [1–3,21]. The SWIM instrument obtains the sea surface mirror and quasi-mirror scattering information at different incident angles by transmitting one nadir beam (0°) and five low incidence beams (2°, 4°, 6°, 8°, and 10°) with rotating scanning. The nadir beam can observe waves similar to the altimeter. The time series of the power of the echoes received by the nadir beam is commonly referred to as a “waveform”. The fundamental parameters such as SWH (i.e., SWHn) are obtained through retracking a typical Brown waveform model [1,2,22]. According to the user’s manual of the satellite, the spatial resolution of SWHn along the orbit is around 70 to 80 km. The off-nadir beams can obtain the modulation information of the wave tilt on the scattering coefficient in multi-azimuths. Combining the information of the nadir beam and the off-nadir beams, the directional wave spectrum can be measured, and the wave parameters such as SWH (SWHs) can be obtained based on the spectrum [1,2].

It is designed so that the SWHn can be used to calibrate the directional sea wave spectra retrieved from the other five rotating beams [3,23]. Spectrometer SWH data have been revised many times by the data publisher [24], and the data quality has been greatly improved compared with the initial version.

In this study, the SWIM_L2_product released by French Centre National d'Études Spatiales (CNES) is appraised in the SCS. From the AVISO platform, the data can be downloaded (ftp://ftp-access.aviso.altimetry.fr/cfosat/, accessed on 2 February 2023). The data from April 2019 to November 2022 are used. The data version number is 5.1.2 before 27 June 2022 and 6.0.0 after that.

2.2. In Situ Observations

Based on the long-term field observation of five representative sites, the performance of the two types of SWH products of the CFOSAT in the SCS is systematically tested. The site location and surrounding terrain are shown in Figure 1, as well as the longitude, latitude, and water depth of each site. Basic information such as observation platform and periods is listed in Table 1. Three of the sites (ST, WS, and DL) are located in shelf waters close to the mainland in the northern part of the SCS, and the other two sites (NS1 and NS2) are located in deep waters in the southern SCS.

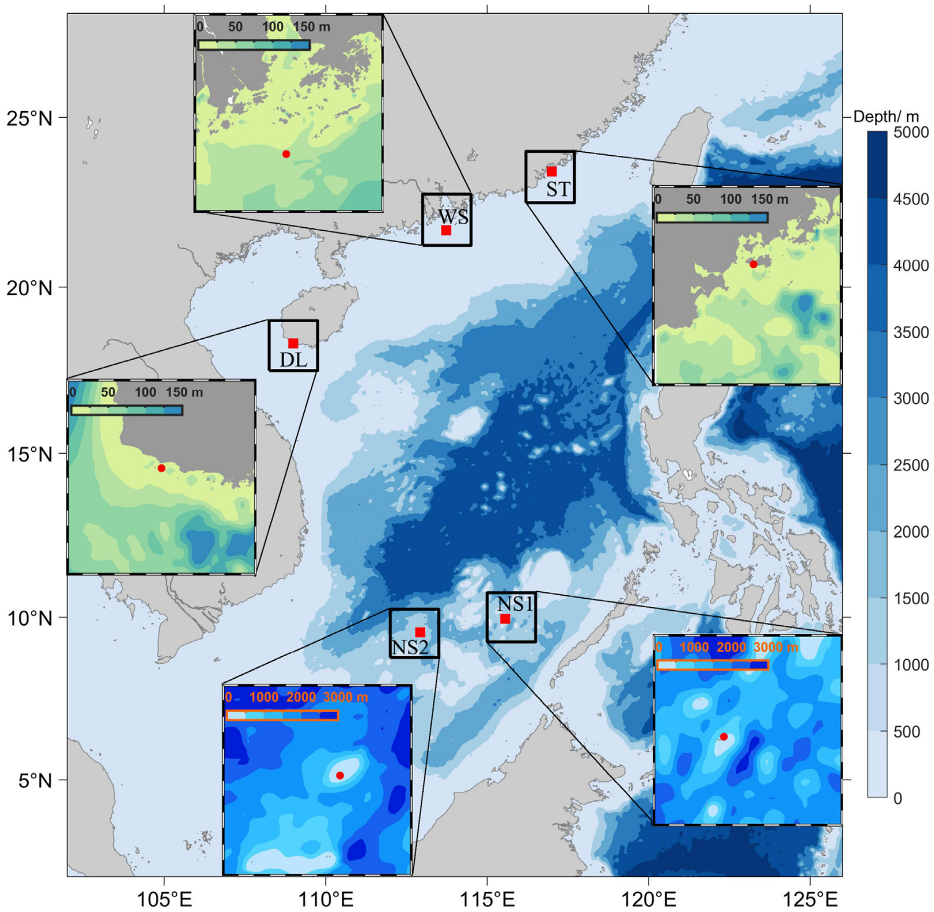

Figure 1. Topography of the South China Sea and the locations of in situ observation sites (in red point) used in this study and their surrounding topography.

Table 1. Information of in situ observation sites.

Site ID	Platform	Wave Sensor	Longitude/Latitude	Depth	Observing Period	Sample Interval
ST	Mooring	AWAC	117°E, 23.42°N	10 m	October 2020–April 2021, June 2021–October 2022	0.5 h
WS	Buoy	Triaxys wave sensor	113.73°E, 21.7°N	37 m	March–October 2022	0.5 h
DL	Mooring	AWAC	109°E, 18.32°N	17 m	January–September 2020, March 2021–June 2022	3 h
NS1	Buoy	Triaxys wave sensor	115.5°E, 10°N	1200 m	November 2018–June 2021 *	1 h
NS2	Buoy	Triaxys wave sensor	113°E, 9.5°N	1240 m	October 2020–October 2021	1 h

* Wave spectrum data of the NS1 site is from November 2018 to July 2020.

The ST and DL sites employed submarine-based observation platforms. In each site, an acoustic wave and current profiler (AWAC) produced by Nortek Co., Norway, was placed on the sea floor. The surface acoustic tracking method is adopted to measure waves by looking upwards. The wave height and wave directions are calculated using the wave spectra. In the WS, NS1, and NS2 sites, buoy platforms equipped with a Triaxys wave sensor manufactured by AXYS Technologies Inc., Canada, were employed to measure waves through the gravity acceleration method. The in situ data used in the present paper include significant wave height, main wave direction, and frequency spectra.

2.3. ERA5 Reanalysis Data

The ECMWF ERA5 reanalysis data, including wind speed at the 10 m level (U_{10}) and wind direction (θ_{wind}), are obtained for auxiliary analysis. ERA5 is the fifth generation ECMWF reanalysis of the global climate and weather [25], providing hourly estimates on single levels for a large number of atmospheric and ocean-wave quantities with a spatial resolution of 0.5°. It can be downloaded from the website http://climate.copernicus.eu/climate-reanalysis (accessed on 2 February 2023).

The data used in this study is from November 2018 to October 2022 covering the observation period of the five in situ sites. The U_{10} and θ_{wind} are interpolated onto each observation site by the bilinear interpolation method, and further interpolated temporally to the measured time of buoy or mooring. Then, they are combined with wave spectrum data to classify the wind sea and swell. Further, the seasonal data are also calculated to describe the meteorological characteristic nearby each site.

2.4. Matching Method of CFOSAT Data and In Situ Observations

To assess the accuracy of the CFOSAT retrievals, the CFOSAT wave data and buoy measurements were collocated in time and space. The criteria of 50 km and 30 min, in many cases, are applied in the altimeter data validation, e.g., [24,26–29]. Some studies take 25 km as a spatial criterion [30]. Under normal circumstances, a space domain ranging from 0 to 150 km and a time domain varying from 0 to 1.5 h are also widely accepted for comparison between the buoy and satellite [31–33].

Comparisons between satellite and field data are complicated by the fact that each of them is measuring different aspects of the temporally and spatially varying field, and hence may differ [26]. The present study chooses a particular spatial window with a radius R = 80 km and a temporal window of 0.5 h to match the CFOSAT parameters with the mooring or buoy data. A neutral space window here is to obtain a potentially large number of spectrometer-buoy collocations for a variable sea condition. The influences of the spatial window radius ranging from 25 to 100 km in the appraisal of COFSAT wave height products are further investigated later.

2.5. The Separation Method of Wind Sea and Swells

Ocean waves usually exist as a mixture of wind sea and swell. To access the accuracy of COFSAT SWH in different sea states, this paper separates the wave samplings into the wind-sea-dominated pattern and swell-dominated pattern. Based on the in situ spectrum data (wave energy according to frequencies) from the sites in deeper water (WS, NS1, and

NS2), the wave pattern is divided by referencing Hanson and Phillips [34]. They introduced the separation frequency to recognize the wind sea from mixed waves in the deep sea. The algorithm of separation frequency is shown in the following:

$$f_S = \frac{g}{2\pi(1.5U_{10}\cos\delta)} \tag{1}$$

where U_{10} is the wind speed of 10 m; δ is the angle between the wind and wind sea, and defined as:

$$\delta = |\theta_{wave} - \theta_{wind}|, \quad \delta \in [0, \pi/2] \tag{2}$$

where θ_{wave} and θ_{wind} are the directions of wave and wind, respectively. The U_{10} and θ_{wind} here are from the ERA5 database. They are interpolated to match the in situ θ_{wave} of each site. Since the wave and wind directions, as well as their differences δ, are continuous at 0 and 2π, it should be $\theta_{wind} = \theta_{wind} + 2\pi$ when $\delta > \pi$ and $\theta_{wind} = \theta_{wind} - 2\pi$ when $\delta < -\pi$.

This relationship defines a separation frequency f_s to distinguish the wind sea and swell. For waves subjected to Equation (2), the partition whose frequency is higher than f_s is considered to be forced by the wind and finally defined as wind sea. All remaining partitions contribute to swell. Waves whose integrated spectrum energy of wind-sea partition is larger than that of swell partition are considered as a wind-sea-dominated pattern and vice versa. Further, waves with δ out of $[0, \pi/2]$ are introduced as the swell-dominated pattern.

3. Results and Discussion

3.1. General Statistics

The scatter diagrams of the comparison between CFOSAT and in situ SWH subjected to a matching window of 80 km × 0.5 h are shown in Figure 2. The statistical parameters are calculated and given in the figure. By comparing with the field observation, it can be found that the quality of CFSAT SWH in the SCS is good. Especially for the far offshore sea area with relatively greater depth, the SWH measured by the CFOSAT has high accuracy. Many studies have also shown good accuracy of altimeter SWH compared with buoy observations in the open ocean, e.g., [35,36]. For the WS, NS1, and NS2 sites, correlation coefficients ranged from 0.74 to 0.97 (mean 0.87), bias ranged from −0.06 m to 0.39 m, and RMSE ranged from 0.36 m to 0.68 m (mean 0.47 m). Studies examining SWIM data found that in earlier releases, such as version 5.1.2 from May 2019 to April 2020, the accuracy of SWHs is not so good at that stage, probably because of the impacts of the high noise level in the spectra [9]. It is noted that the error of SWHs and the error of SWHn are generally similar compared to the in situ observations, and there is no significant difference in accuracy between the SWHs and SWHn in today's version (Figure 2), indicating that the latest version of the wave spectra products from SWIM has been well corrected. Compared with the data in the deep water, however, the satellite SWH deviates greatly from the in situ observing value for the sites in shallow water near the coast. Especially for the ST site, which is too close to the coast, the satellite-observed value is generally greater than the field-observed value.

In general, the accuracies of SWHs and SWHn are similar. For instance, in the NS1 site that gathered the most SWIM-buoy collocation, the bias, RMSE, scattering index (SI), and correlation coefficient (r) of SWHs is 0.17 m, 0.36 m, 0.32, and 0.89, and those of SWHn are 0.20 m, 0.37 m, 0.32, and 0.90. The similar SI and r values for SWHs and SWHn show the consistency of COFSAT SWH and buoy data. The statistical parameters of COFSAT SWH in other sites except for WS also present a similar result. For the WS site, the bias of SWH in nadir mode is significantly smaller than that of SWHs, while the RMSE, SI, and r are larger than the one in spectrometer mode. The potential reason is sampling capacity in WS is relatively small, which introduces uncertainty in error appraisal. What is more, the sampling period is during late spring to early autumn when the frequency of typhoons, as well as extreme waves, is high. As a result, further study should pay attention to the appraisal difference between the SWHn and SWHs resulting from sampling uncertainty.

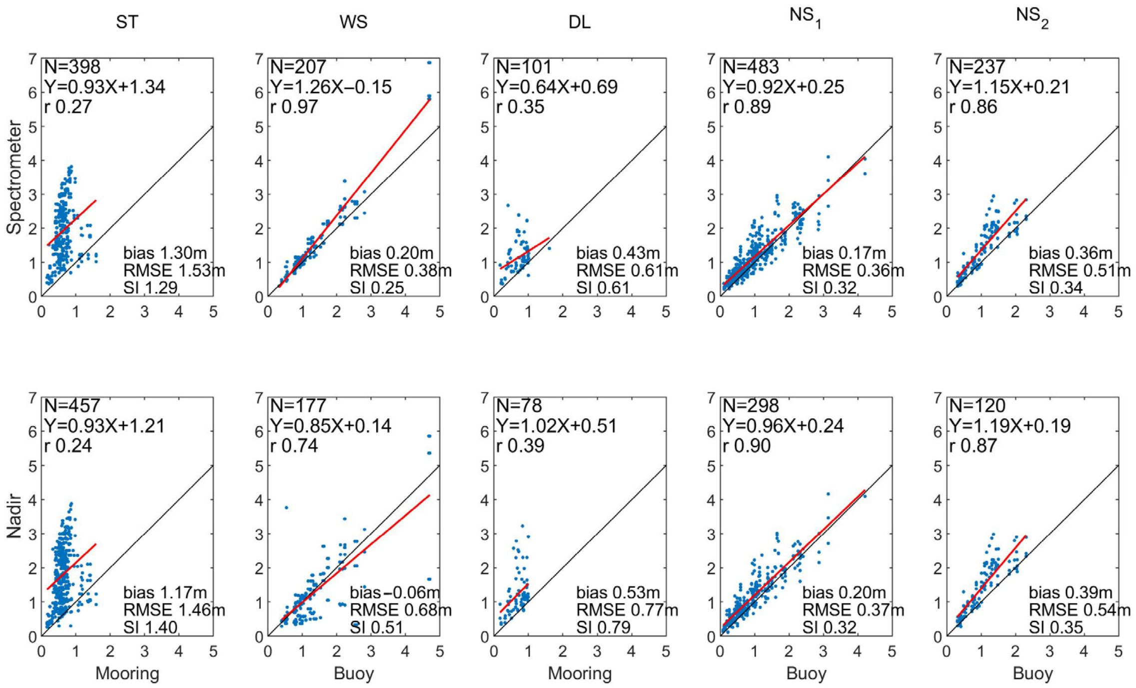

Figure 2. Scatter comparison of spectrometer significant wave height (SWHs) and nadir SWH (SWHn) measured by the CFOSAT with the in situ observations at the five sites, whose information is shown in Figure 1 and Table 1. The statistical parameters of bias, root-mean-square error (RMSE), scattering index (SI), and correlation coefficient (r), are calculated following the methods by Yang and Zhang [30].

There is a large deviation between the satellite and the field observations in the sea area near the coast. One of the reasons may be the high dynamical variability of the nearshore wave itself, and the incompatibility of the remote sensing points and the field observation points. Under the influence of shorelines, the spatial differences and variation rules of nearshore wave elements may be very complicated [37,38], and the 80 km × 30 min spatial-temporal window matching scheme adopted in this study is difficult to effectively match the two observations. In this study, the influence of different matching scales on the calculation results of error indicators is evaluated by adjusting the radius of the space-matching window (Figure 3). The influence of radius selection on the calculation results of error indexes is not significant in the sea area where most sites are located. On the one hand, this result further verifies the robustness of the high-precision analysis results of CFOSAT SWH. On the other hand, it is also found that when the matching radius decreases to 25 km, the data capacity that can be matched by each site is very small. Therefore, the results of this study do not question the quality of the satellite telemetry, especially in offshore waters, but point out the need to construct a more scientific and reasonable matching method.

With different matching radiuses, scattering patterns of SWHn compared with the in situ observations in the shelf waters close to the mainland are illustrated in Figure 4. For the shallow sites of ST and DL, smaller errors are suggested with decreased matching radius. However, the inaccuracy partitions (red cycles in Figure 4) do not disappear in a tiny radius of 25 km, suggesting the main source of the incorrect value is not contributed from the spatial matching criteria. There are robust errors in the shallow water in sites too close to the land. On the contrary, for the WS site relatively far from the land, the decreasing radius continuously leads to a smaller error excluding the abnormal value. When the radius is 10 km, the error indicators of this site would be further improved with a bias of −0.05 m and an RMSE of 0.20 m.

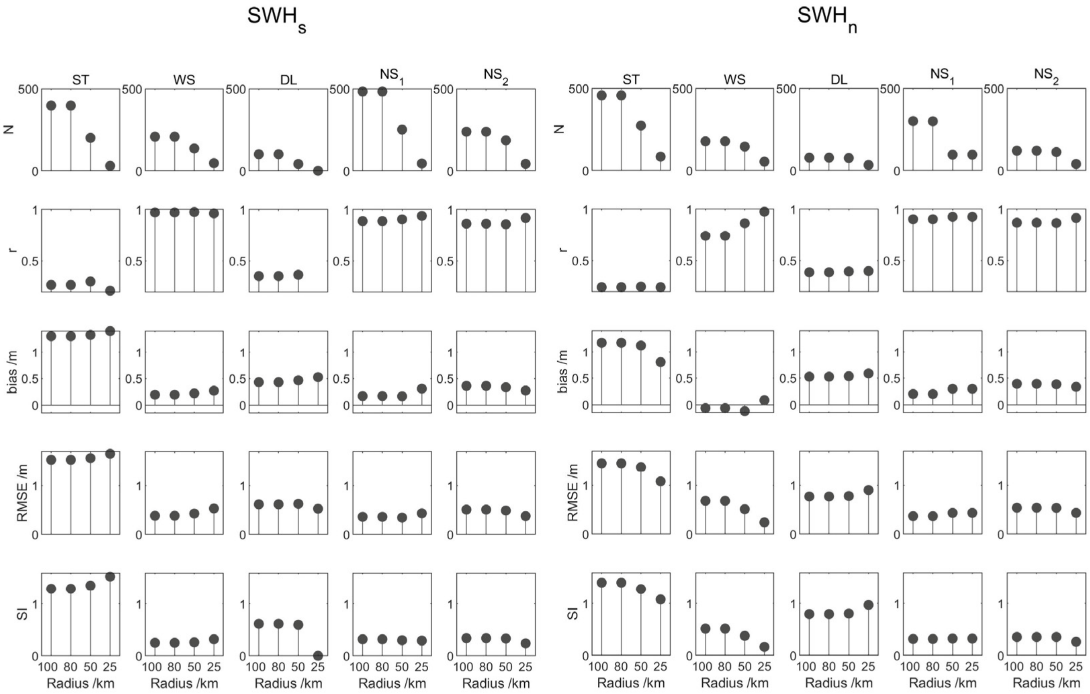

Figure 3. Variations of the amount of the matched samples (*N*), correlation coefficient (*r*), bias, root mean squared error (RMSE), and scatter index (SI) for spectrometer SWH (SWHs) and nadir SWH (SWHn) with matching radius.

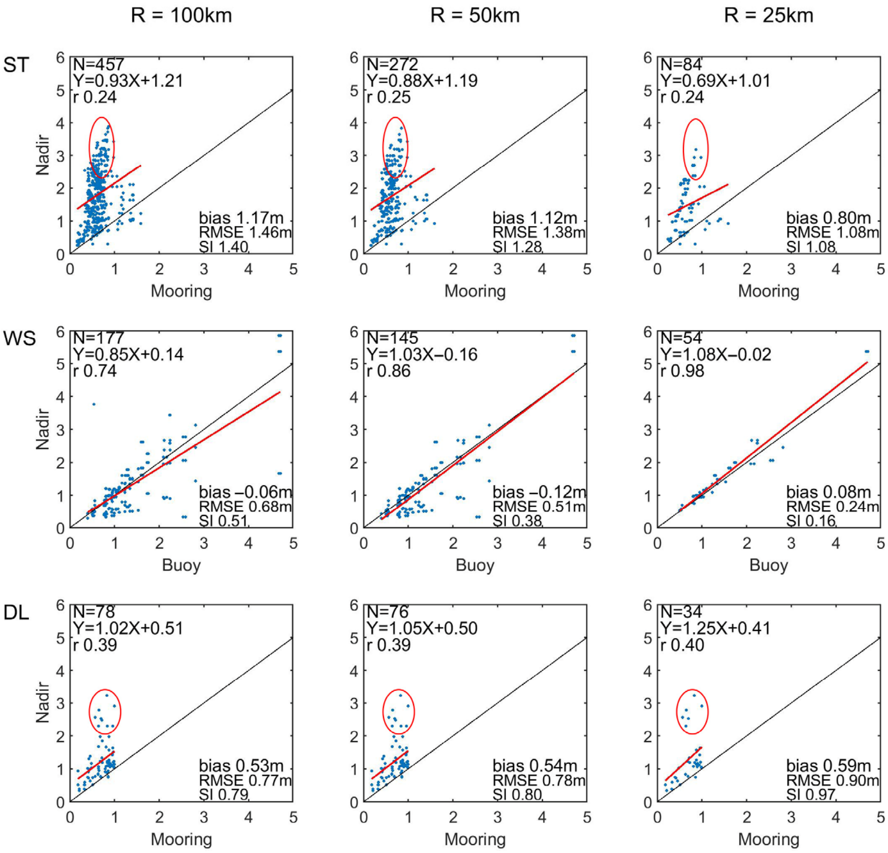

Figure 4. Scatter comparison and related error indexes of nadir SWH measured by the CFOSAT with the in situ observations at the nearshore sites (ST, WS, and DL) with different matching radiuses.

3.2. Contamination of Rain and Land

Land and rainfall are the important pollution sources of remote sensing image information. For example, under the impacts of rainfall, the accuracy of satellite data will often decrease obviously [29]. In addition, the accuracy of SWH may be degraded near the coast due to the reflections from the land and the calm water pollution [22,39]. For this reason, this study specially analyzed and compared the difference in error indicators of CFOSAT SWH data in the case of rainfall or land scenarios. The analysis results show that, in the open seas sites (NS1 and NS2), the error indexes of the CFOSAT SWH are improved in the rain-free situation compared to that in the rainy situation (Table 2). For the nearshore sites, reduced RMSE and bias appear in the WS and DL sites when the land contamination is filtered out (Table 3). Thus, the contamination of rain and land may affect the data accuracy of the CFOSAT.

Table 2. Error indexes of CFOSAT SWH at the five in situ sites under rain and rain-free scenarios.

	ST		**WS**		**DL**		**NS1**		**NS2**	
	Rain Free	**Rain**	**Rain Free**	**Rain**	**Rain Free**	**Rain**	**Rain Free**	**Rain**	**Rain Free**	**Rain**
N	384	14	196	11	96	5	466	17	221	16
r	0.27	0.16	0.97	1.00	0.34	/	0.89	0.74	0.86	0.83
Bias (m)	1.30	1.30	0.20	0.16	0.42	/	0.17	0.18	0.36	0.45
RMSE (m)	1.54	1.51	0.39	0.18	0.62	/	0.36	0.38	0.50	0.53
SI	1.29	1.32	0.26	0.06	0.62	/	0.32	0.28	0.35	0.21

Table 3. Error indexes of CFOSAT SWH at the five in situ sites under land and land-free scenarios.

	ST		**WS**		**DL**		**NS1**		**NS2**	
	Land Free	**Land**	**Land Free**	**Land**	**Land Free**	**Land**	**Land Free**	**Land**	**Land Free**	**Land**
N	177	221	103	104	75	26	483	0	237	0
r	0.29	0.25	0.97	0.97	0.32	0.42	0.89	/	0.86	/
Bias (m)	1.33	1.28	0.18	0.21	0.43	0.44	0.17	/	0.35	/
RMSE (m)	1.54	1.53	0.34	0.42	0.60	0.65	0.36	/	0.51	/
SI	1.25	1.32	0.23	0.27	0.59	0.68	0.32	/	0.34	/

It is worth noting that although the existence of land can be well identified, the changes in waves caused by the shoreline and shallow topography may not be fully considered, which may be an important reason why satellite measurements deviate from the measured values in nearshore waters, as shown in Figure 2. During waves traversing shorelines and shallow water terrain, shallowing, refraction, diffraction, and other deformation processes will occur [13,18,19]. Coastal waves usually cannot be directly interpreted by the standard model suitable for the situation in the open oceans [22]. However, the accuracy of data sets for identifying land factors is not higher than that of data sets without land factors (Table 3). It can be seen that the coastal process has not been considered in satellite data inversion algorithms. Therefore, the closer the sites are to the coast and the shallower water, the greater the influence of coastal factors on wave dynamics, so the deviation from measured values is obvious. The differences in location and error indices of the WS, DL, and ST sites illustrate this well: they are about tens of kilometers, several kilometers, and hundreds of meters away from the coast, and their water depths are more than 30 m, close to 20 m and about 10 m, respectively (Figure 1 and Table 1); their r indices show an obvious decline, while bias and RMSE and other indices show an obvious increasing trend accordingly (Figure 2 and Table 3).

3.3. Effects of Different Sea States

Further analysis of the SWH errors with wave height, period, and swell proportion shows that the satellite data quality is relatively better in high sea conditions with high swell proportion (Figures 5 and 6). The deviation of the SWHs increases first and then decreases with the increase of wave height, which is consistent with CFOSAT SWH performances reported by Liang et al. [40]. They suggested the SWHn shows a smaller error in the wave height within 2–3 m. Especially for the relatively open sea areas where the WS, NS1, and NS2 sites are located, when SWH is larger than 2 m, the relative error of the SWH data of CFOSAT, whether SWHs or SWHn, is lower than that when SWH is less than 2 m (Figure 5). It has also been shown by previous studies that the accuracy of remote sensing wave observation is generally better in high sea states than that in low sea states, which is due to the higher homogeneity of wave propagation compared to high sea states [7]. The analysis results in this paper are consistent with the existing results.

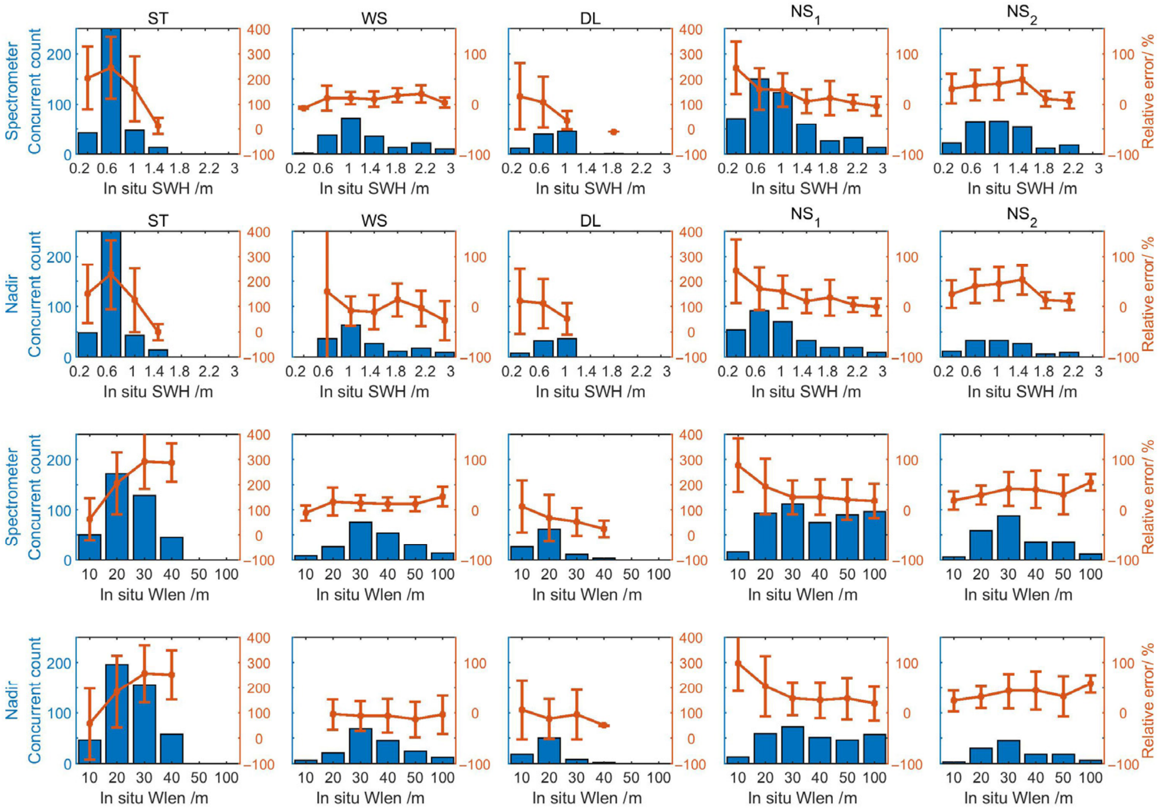

Figure 5. Relative error of the CFOSAT SWH compared to in situ observations at the five sites, in functions of in situ SWH and mean wavelength (Wlen). The left labels indicate the concurrent counts of the CFOSAT and in situ SWH, while the right ones are relative errors of CFOSAT SWH with error bars.

In addition, the analysis results emphasize the importance of the swell proportion for the quality of SWH data. According to the wave measurement method, CFOSAT is better at observing fully developed swell whose wavelength is relatively long [3,7]. The verification of the satellite data that has been carried out is more aimed at the global open oceans, such as the northeast of the Pacific Ocean and the northwest of the Atlantic Ocean, e.g., [4,6,9]. By contrast, the SCS has a relatively closed and more complex topography, and the wavelengths observed by the sites are mostly lower than 50 m, which indicates that the proportion of swell is significantly lower than in the open oceans [15–17]. This difference determines that the accuracy of the data in the SCS cannot directly apply to the previous evaluation conclusions for global open oceans.

Further analysis of the wave spectrum data at the observation sites is performed to distinguish whether the sea state is dominated by swell or wind sea energy. It can be found that in the sea state dominated by the swell, compared with the sea state dominated by the wind sea, the satellite-measured SWH better matches the in situ observations (Figure 6).

It shows that when applying the wave data of CFOSAT to the SCS and other areas with relatively complex topography and shoreline environments, we should pay special attention to the influence of factors such as the proportion of swell energy. SWIM data itself can provide wave spectra, and making full use of this data to obtain information on swell proportion is expected to further optimize the quality of data in such sea areas.

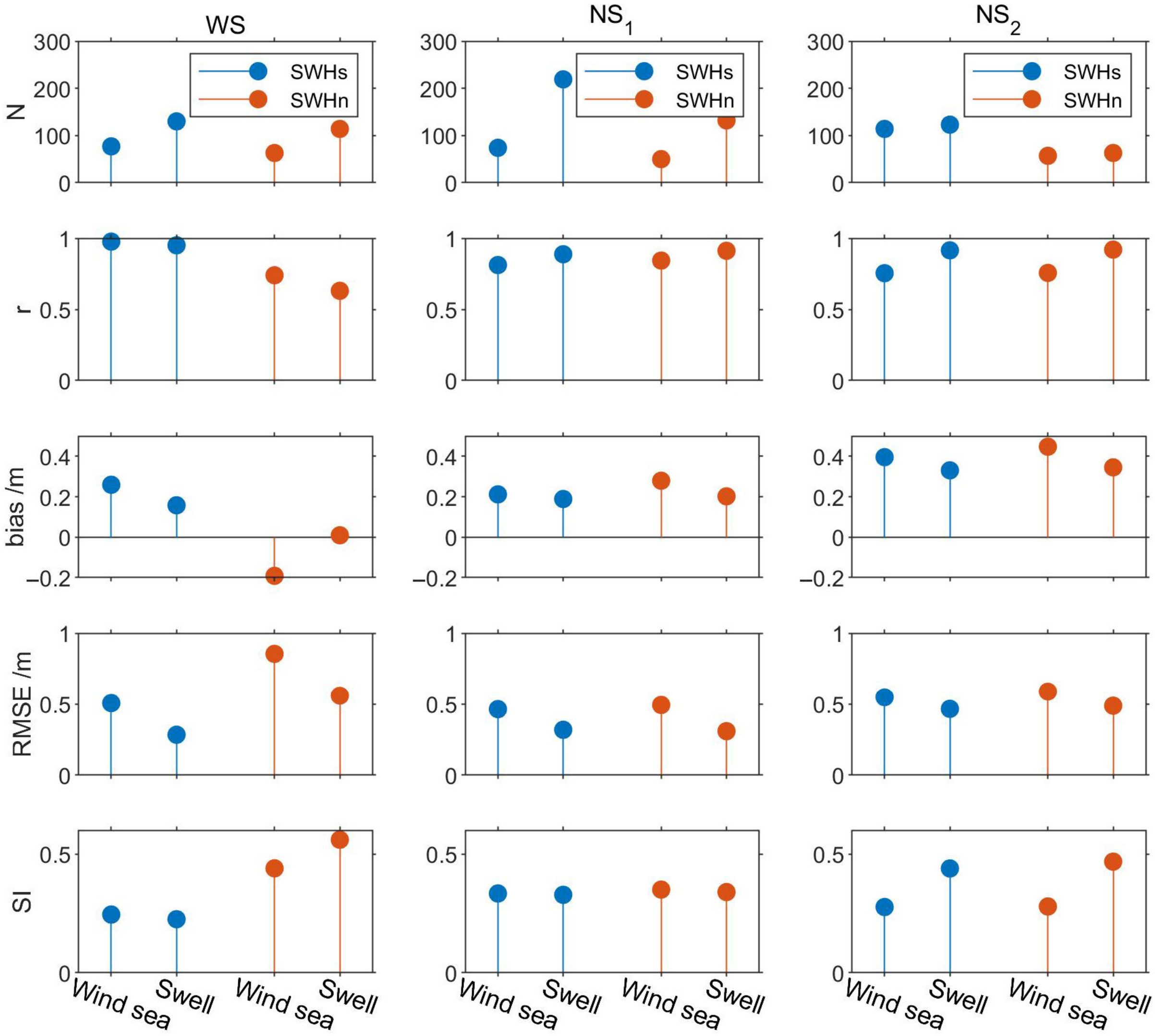

Figure 6. Comparison of the amount of the matched samples (N), correlation coefficient (r), bias, root mean squared error (RMSE), and scatter index (SI) between wind-sea-dominated and swell-dominated sea states, for the WS, NS1, and NS2 sites.

3.4. Seasonal Variations Associated with Topographical Influence

The wind field in the SCS is dominated by the monsoon with the northeast wind in winter and early spring and the southwest wind in summer [12]. The wave field presents a more complex seasonal variation characteristic. On the one hand, the seasonality of the wave varies under the drive of monsoon; on the other hand, the local waves are mixed with the swell spreads throughout the SCS basin, which is deformed through the shallow water topography of islands and reefs [5]. As the wave is transmitted from the deep sea to the shallow water, its energy would be reduced and its propagation direction would be deflected by the bottom friction or land blocking [34–36]. Such coupling effect of monsoon and topographic factors determines the seasonal differences in deviation of the CFOSAT SWH in different regions of the SCS (Figures 7–11).

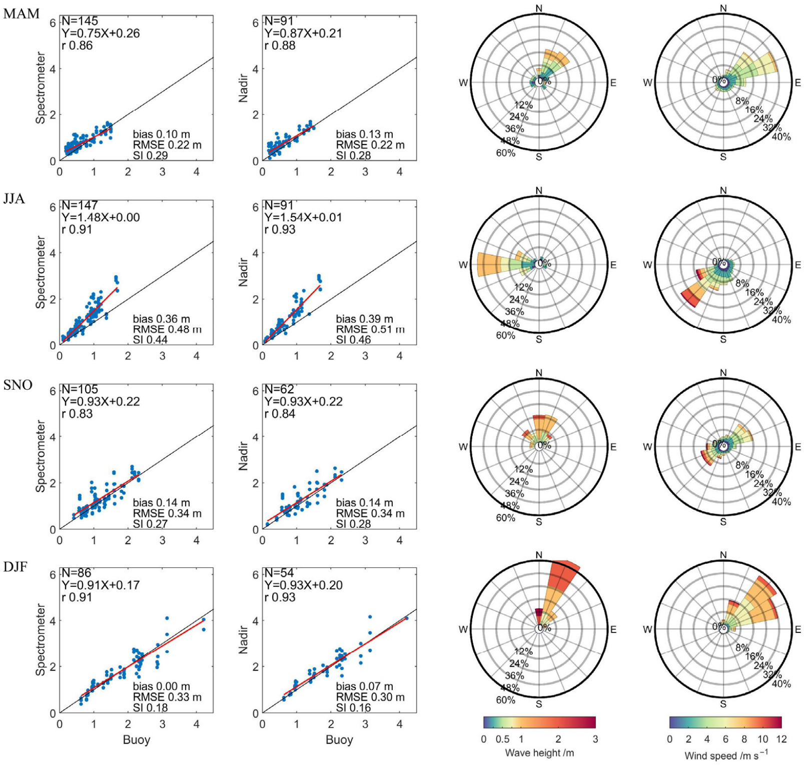

Figure 7. Seasonality of the scatter plot comparing CFOSAT and in situ SWH, and rose charts of wave and wind at the NS1 site. The left half is scattered diagrams of the spectrometer SWH and nadir SWH versus in situ observation during spring (MAM), summer (JJA), autumn (SON), and winter (DJF). The right half is wave rose and wind rose of the corresponding seasons.

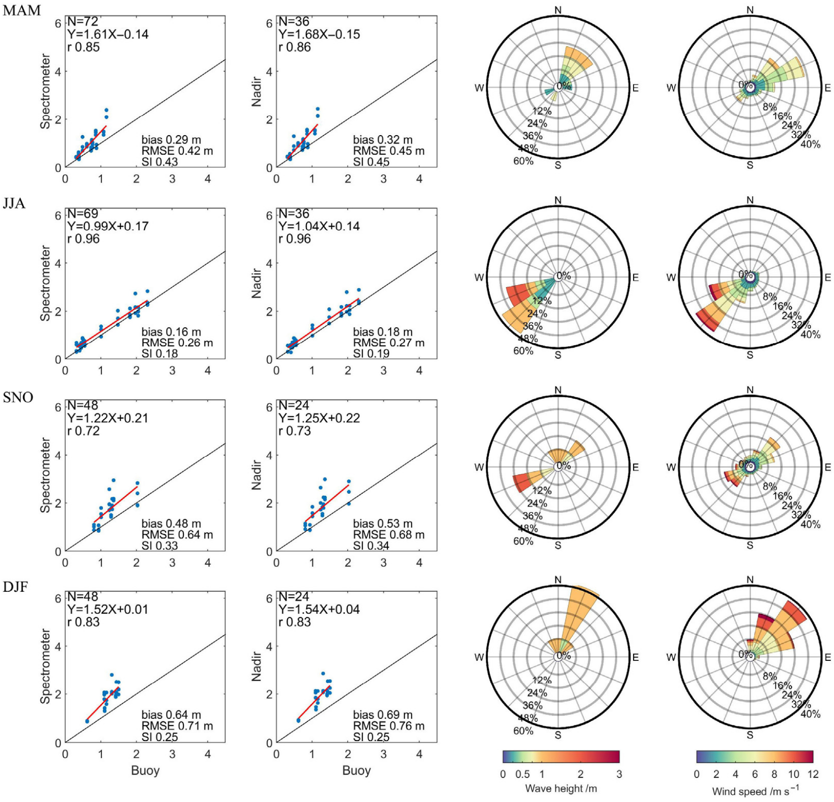

Figure 8. Same as Figure 7 but for the NS2 site.

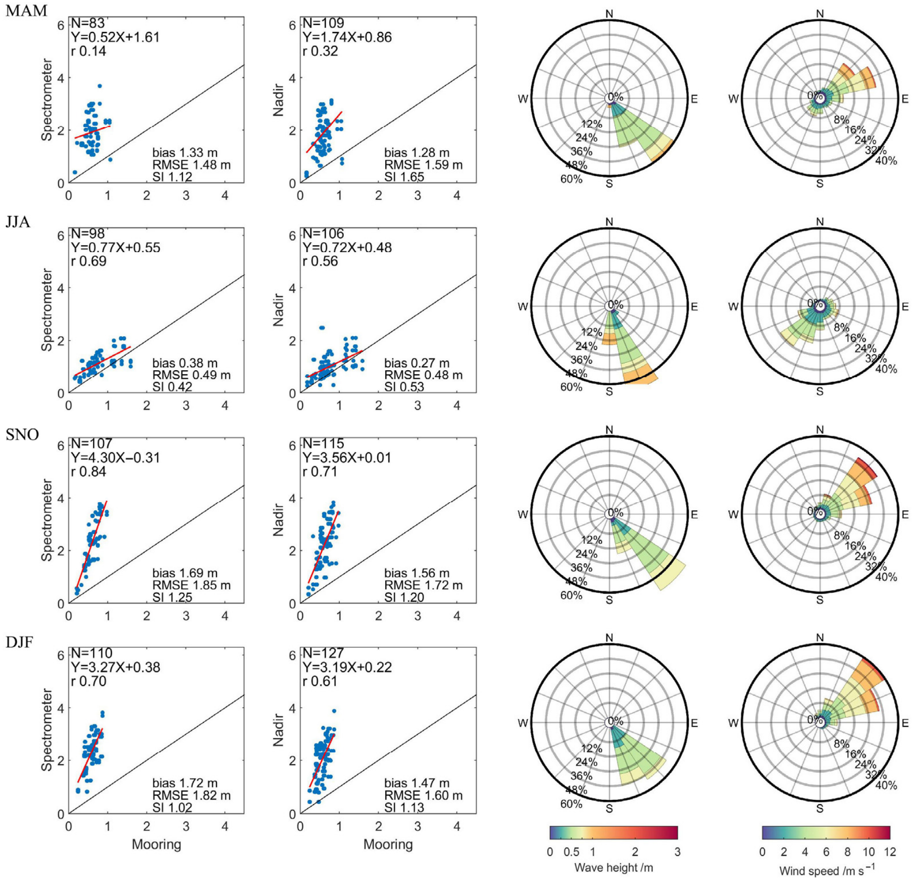

Figure 9. Same as Figure 7 but for the ST site.

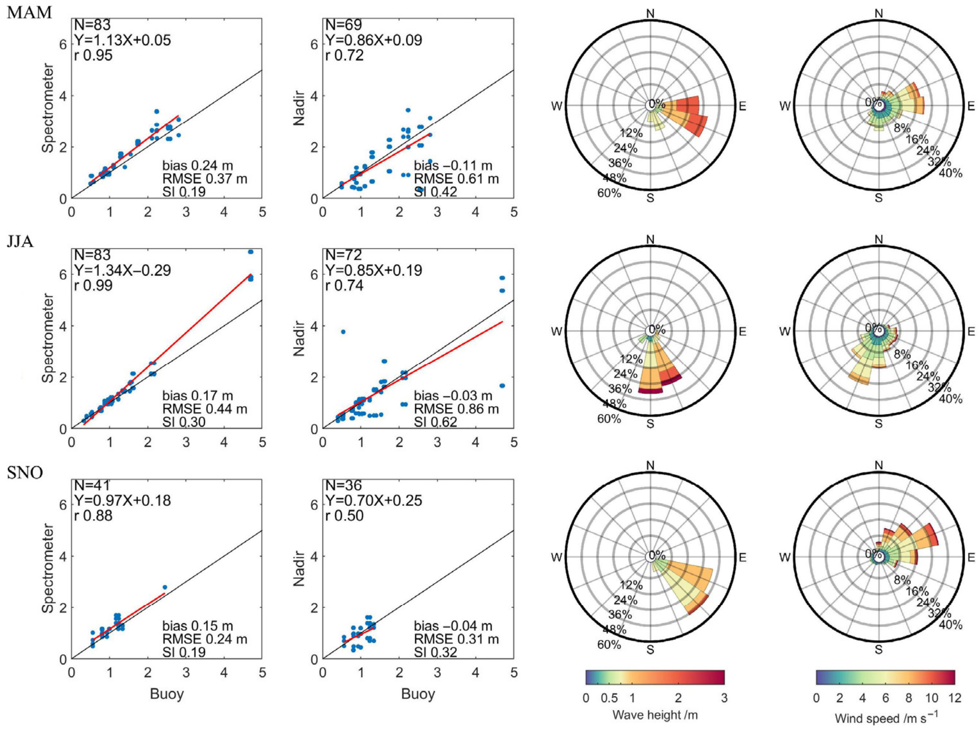

Figure 10. Same as Figure 7 but for the WS site. The season when the sampling capacity of collation data is less than 20 is not shown.

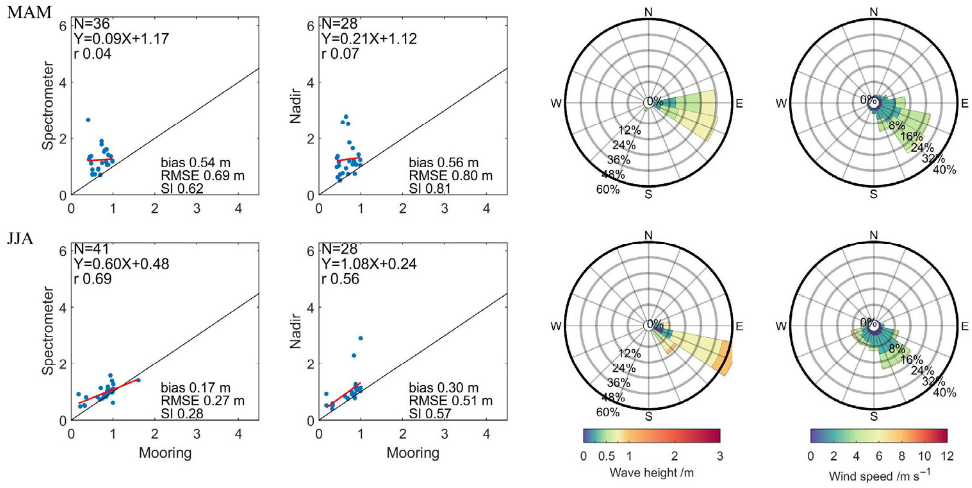

Figure 11. Same as Figure 7 but for the DL site. The seasons when the capacity of matched samples is less than 20 are not shown.

3.4.1. Sites in Relatively Open Areas

For the sea area in the southern SCS far away from the mainland (such as the NS1 and NS2 sites in Figures 7 and 8), the wave direction and wind direction in the four seasons are the same because they are not affected by the land (Figure 1 and Table 3). The overall accuracy of the CFOSAT SWH in these two sites is much better than the two inshore sites of ST and DL (Figure 2). However, due to the numerous islands and reefs in this area, the wave propagation process may still be influenced by the shallow water topography. If such topographic factors are not effectively calibrated and the inversion algorithm for the fully open ocean is still used, the quality of satellite data here is also vulnerable.

According to the underwater topographic map around the site, it can be found that the north area of the NS1 site is relatively open, while there are more reefs in its southwest direction (Figure 1). As a result, waves from the north are largely unhindered from autumn to spring, while waves from the west during the summer monsoon have to overcome the shallow terrain of islands and reefs, resulting in a weaker agreement of the SWH between CFOSAT and buoys in summer than that in other seasons (Figure 7).

In contrast, the southwest side of the NS2 site is relatively open while its northeast side has more islands and reefs. During the summer monsoon, waves from the southwest can reach the site without being hindered, while during the other seasons, waves from the northeast need to pass through the shallow water terrain of islands and reefs. Therefore, the accuracy indicators of the sea area where the NS2 site is located in summer are better than that in other seasons (Figure 8). It can be seen that, in the absence of targeted calibration, the coupling effect of monsoon and topography may lead to seasonal and regional fluctuations in the quality of satellite data.

3.4.2. Sites in Nearshore Areas

As for the sites in the northern part of the SCS (ST, WS, and DL) close to the mainland, the trap and shelter effects of topography on waves lead to the wave direction being stable throughout the year, mostly between 90° (E) and 180° (S) (Figures 9–11). This results in a situation where the wind direction from autumn to spring is not consistent with the direction of the wave transmitted nearby each site. In the process of wave generation and propagation, the mainland coastline plays an obvious shielding role: southward waves need to bypass the topographic barrier for long-distance travel, experiencing more subtracting effects of shallow water before they approach the nearshore sites. Considering the rough orbital resolution of 70–80 km and the large sampling area of 70 km × 90 km [1,2], the satellite observations corresponding to the nearshore sites may reflect the situation of the relatively open areas that would be far away from the site. Therefore, the wave climate represented by in situ observations and satellite data may differ, which leads to the difference in their SWH values. The effect of shoreline and topography becomes more pronounced when close to the shore, resulting in large deviations in wave remote sensing. This is most evident at the DL and ST sites, which are only a few kilometers and a few hundred meters offshore, respectively (Figures 9 and 11).

For instance, in the ST site, the wave direction does not show a significant seasonality as the wind (Figure 11). It is suggested that the inshore waves are strongly affected by topography. For the trapped effect of the continental shoreline, wave propagation direction here is stable throughout the year, always from southeast to northwest. Despite this, during the summer, the waves from south and south-southeast increase. That is, driven by the southwest monsoon, the waves spread to the site from the open seas do not experience too much topographic obstruction, resulting in a good agreement between satellite and field observations. Figure 2 shows that most SWH data are smaller than 1 m; it is found that most considerable in situ SWH samples exceeding 1 m mainly appear in summer. Although the overall accuracy of satellite SWH is not ideal, at this site, the error indicators in summer are greatly improved.

Compared to the ST site, the wave rose at the WS site shows a more distinct seasonality. There are obvious signs of southward drift of wave directions in summer (Figure 9). A potential reason is that the WS site is farther from the mainland coast than the ST site, greatly reducing the capture effect of the coast on wave direction. Moreover, with the break of the SCS monsoon in summer, the expected improvement of the CFOSAT SWH at this site does not appear. It should be noted that the considerable errors in this season may result from the data accuracy of SWH larger than 3 m. The occurrence frequency of such extreme waves significantly increases during summer, and the high sea surface roughness may affect the sea surface emissivity, introducing deviations in the retrieval algorithm of SWH.

The CFOSAT SWH during spring and summer at the DL site are compared in Figure 11. Similar to the situation in ST, during the monsoon period in summer, the southeasterly wind slightly shifts southward, and so do the wave directions. As the partition of southeasterly waves increases, the topographic obstruct becomes weak, and the accuracy of the CFOSAT SWH is improved. Generally speaking, however, the seasonal variation of satellite data accuracy at the DL site is not as significant as that at the ST site. The latter site is too close to the land, resulting in a significant influence on wave propagation by the topography, thus greatly affecting the satellite wave measurement accuracy.

3.5. Coastal Shallow Water Effects besides Land Shelter

Apart from the shelter effects of land, coastal waves will also be affected by shallow topography, resulting in complex deformation, thus affecting the observation accuracy of the satellites. For the nearshore sites such as ST and DL when the wind and wave propagate essentially in the same directions, the wave propagation process will be largely free from the shielding effect of the northern mainland. Thus, different ranges of the included angle formed by wind direction and wave direction (δ) are extracted from the data of the two sites and repeated statistics of the error indicators within the ranges. The results show that the error indexes such as bias and RMSE appear as upward trends with the increase of the angle (Figure 12). If the data on the relative consistency of wave direction and wind direction are compared with the data on the relative deviation of wave direction and wind direction, the error-index of the former will be significantly smaller (see the second and the last rows in Figure 12). It implies that if the land shelter effect can be removed, the coincidence between the observation data of nearshore stations and satellite data will be improved, which further verifies the phenomenon clarified in Section 3.4.2 of the influence of the land shelter on the data performances. However, it should be pointed out that even if the wave direction is consistent with the wind direction, the deviations of SWH measured by satellites from the field observations are still higher than those of the NS1 and NS2 stations, by comparing the two right panels in Figure 2 with the second and the last raw data panels in Figure 12. Especially for the DL station, since waves mainly come from the east, consistent with the wind direction for most of the time, and the shelter effect by the northern shoreline is relatively limited, while the coincidence between satellite and in situ observations is still obviously worse than those of the NS1 and NS2 stations. Such results indicate that even if the shielding effect of the continental shoreline is excluded, the waves are still affected by shallow factors.

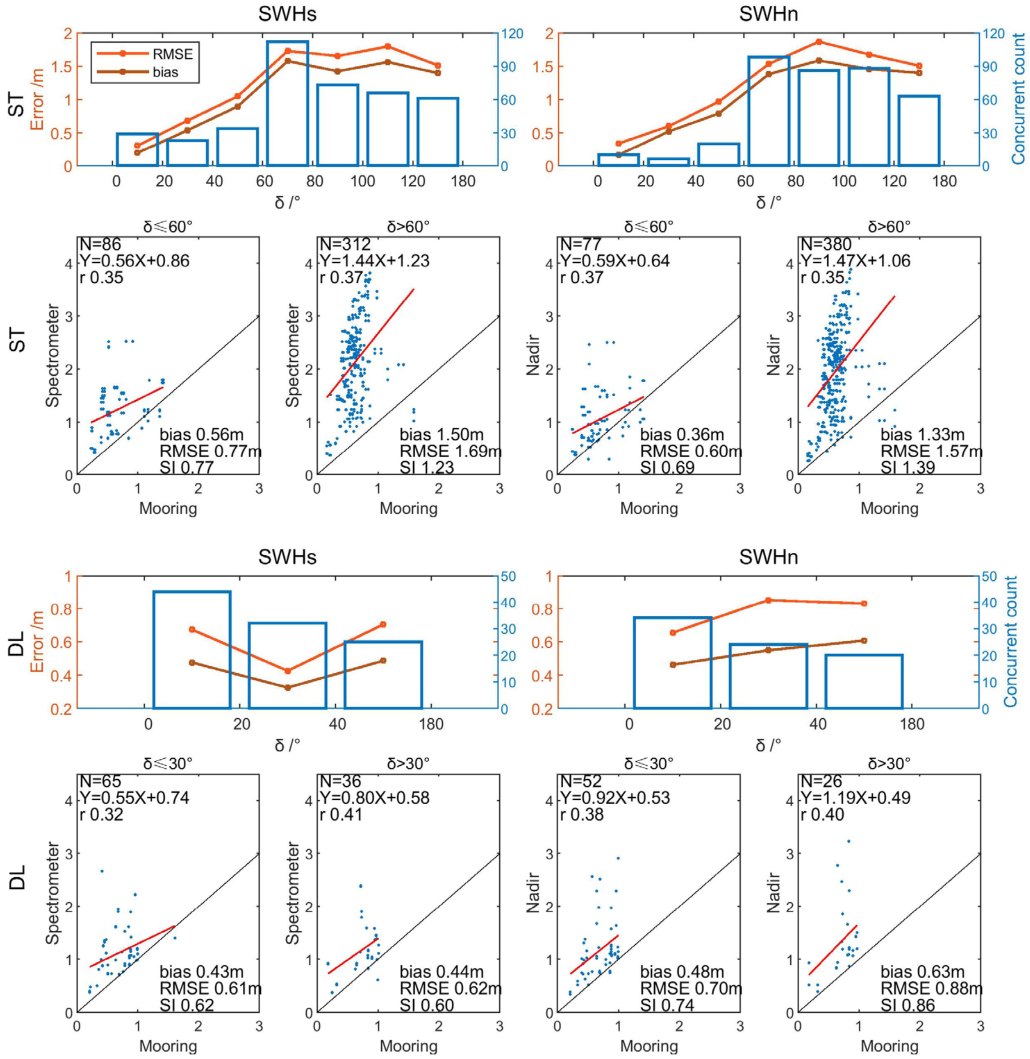

Figure 12. Error indexes as functions of the angle between the wind and wave directions (δ) and comparison of scatterplots of CFOSAT SWH versus mooring observations at the nearshore sites (ST and DL) between smaller δ and larger δ. Threshold δ values of 60° and 30° are adopted for ST and DL sites, respectively, according to their actual wave climates.

The shallow water effects may have negative impacts on the performance of CFOSAT observations in nearshore areas in two ways. Firstly, for SWHn, the raw data provided by nadir altimeters onboard satellite missions are processed to remove unwanted instrumental effects [41]. Although the contamination from land and surface reflections [42] seems to have been well-considered in the data processing of CFOSAT (Section 3.2), the less relevant geophysical corrections in coastal regions than in open oceans [41,43] are still an essential issue that needs to be handled. For example, the nearshore wave undergoes shoaling, refraction, diffraction, and other deformations influenced by shallow topography [13,18,19], which can lead to the sea state responses to atmospheric forcing different from those in the open oceans. This may cause the algorithm developed for open ocean to fail in the nearshore areas. Secondly, for the observation of SWHs, the SWIM's low-incidence normalized radar cross-section is mainly sensitive to the sea surface tilt corresponding to the long wave (70–500 m wavelength) [1–3]. Meanwhile, the waves in the coastal areas are usually affected by the shallow topography, and rarely have a long wavelength, which deviates too much from the design standard of the SWIM instrument. Assuming the waves are fully developed, conventional inversion algorithms for open oceans are usually limited in their applicability to coastal waves.

In other words, both SWHn and SWHs need to fully consider the wave propagation and transformation in the nearshore areas when constructing appropriate algorithms for inversion and post-processing of satellite-measured raw data into SWH products. Otherwise, routine algorithms designed for open oceans would easily lead to the deviation of SWH data from the in situ observations in nearshore areas.

4. Conclusions

Using the long-term continuous in situ observation data from five typical sites, the performance of China–France Oceanography Satellite (CFOSAT) significant wave height (SWH) data in the South China Sea (SCS) is systematically evaluated, and the factors affecting the data quality are analyzed. Our results mainly include two findings: First, the data quality of CFOSAT is generally good in the SCS. The average correlation coefficient is as high as 0.87, and the average root-mean-square error is 0.47 m in the relatively open and deep areas of the SCS. The accuracy of the spectrometer SWH is equal to that of the nadir SWH, with some indexes at certain sites being better. The SWIM data before 27 June 2022 will be reprocessed officially to complete the latest 6.0.0 version soon, a better quality SWH data can be expected in the future.

Second, unique environmental factors such as coastlines, topography, and monsoons may lead to errors in the satellite data in certain cases. Seasonal wind fields drive waves to propagate in different directions throughout the SCS. During the propagation, the waves in the southern SCS with relatively deep water may be affected by a large number of dotted reefs, leading to wave deformations and energy dissipation. In the nearshore areas, waves tend to be sheltered by the mainland or distorted by the shallow topography effects. All these processes may lead to a low proportion of swell energy and swell occurrence probability due to the difficulty in the full development of swell. The low proportion of swell is a disadvantage for the CFOSAT spectrometer to effectively observe or invert the wave data and may result in possible errors.

Although the data validity of CFOSAT has been widely verified in relatively open oceans with fully developed swells, such as the Pacific Ocean and the Atlantic Ocean, in fact, many local important sea areas still lack sufficient verification against in situ observations. In the SCS, a relatively enclosed sea with densely distributed reefs, the development of swell may be limited, and it is easy to be affected by coastlines or topography, resulting in complex variations. In conclusion, this study provides technical support for the application of the CFOSAT data in the SCS and emphasizes the importance of data calibration and verification when applying the data in specific local seas. Improved methods for obtaining more accurate wave data for shallow areas affected by complex terrain, e.g., with a consideration of the different impacts by when the satellite is flying onshore and offshore, will be expected in the future.

Author Contributions: Conceptualization, B.L. and J.L. (Junmin Li); methodology, B.L.; validation, B.L. and P.S.; formal analysis, B.L.; investigation, J.L. (Junliang Li), B.L. and W.C.; resources, S.T.; data curation, S.T.; writing—original draft preparation, B.L.; writing—review and editing, J.L. (Junmin Li); supervision, J.L. (Junmin Li); project administration, J.L. (Junmin Li); funding acquisition, J.L. (Junmin Li), B.L. and P.S. All authors have read and agreed to the published version of the manuscript.

Funding: This research was funded by the National Key Research and Development Program of China (2022YFC3103605), the Hainan Provincial Natural Science Foundation of China (421QN380), the Guangzhou Science and Technology Project (202102020464), the Science and Technology Projects of Guangdong Province (2021B1212050023), the development fund of South China Sea Institute of Oceanology of the Chinese Academy of Sciences (SCSIO202207), and the CAS Key Laboratory of Science and Technology on Operational Oceanography (OOST2021-02).

Data Availability Statement: The CFOSAT wave data are downloaded from the AVISO platform (ftp://ftp-access.aviso.altimetry.fr/cfosat/, accessed on 2 February 2023). The ERA5 hourly single levels data are downloaded from Copernicus Climate Data Store (http://climate.copernicus.eu/climate-reanalysis/, accessed on 2 February 2023). The buoy and mooring data are available from the corresponding author by request.

Acknowledgments: The calculations in this study are supported by the High-Performance Computing Division in the South China Sea Institute of Oceanology. The buoys at the observation sites were deployed by R/V Shiyan 6. We thank all the crew for their help during the cruise.

Conflicts of Interest: The authors declare no conflict of interest.

References

1. Tison, C.; Hauser, D. SWIM Products Users Guide: Product Description and Algorithm Theoretical Baseline Description. 2018. Available online: https://www.aviso.altimetry.fr/fileadmin/documents/data/tools/SWIM_ProductUserGuide.pdf (accessed on 2 February 2023).
2. Hauser, D.; Tourain, C.; Hermozo, L. Report on the SWIM cal/val at the End of the Verification Phase. 2019. Available online: https://www.aviso.altimetry.fr/fileadmin/user_upload/SWIM_CalvalReport_compressed.pdf (accessed on 2 February 2023).
3. Hauser, D.; Tourain, C.; Hermozo, L.; Alraddawi, D.; Aouf, L.; Chapron, B.; Dalphinet, A.; Delaye, L.; Dalila, M.; Dormy, E.; et al. New observations from the SWIM radar on-board CFOSAT: Instrument validation and ocean wave measurement assessment. *IEEE Trans. Geosci. Remote* **2021**, *59*, 5–26. [CrossRef]
4. Wang, J.K.; Aouf, L.; Dalphinet, A.; Li, B.X.; Xu, Y.; Liu, J.Q. Acquisition of the significant wave height from CFOSAT SWIM spectra through a deep neural network and its impact on wave model assimilation. *J. Geophys. Res. Oceans* **2021**, *126*, e2020JC016885. [CrossRef]
5. Wang, J.K.; Aouf, L.; Dalphinet, A.; Zhang, Y.G.; Liu, J.Q. The wide swath significant wave height: An innovative reconstruction of significant wave heights from CFOSAT's SWIM and scatterometer using deep learning. *Geophys. Res. Lett.* **2021**, *48*, e2020GL091276. [CrossRef]
6. Jiang, H.; Song, Y.; Mironov, A.; Yang, Z.; Xu, Y.; Liu, J. Accurate mean wave period from SWIM instrument on-board CFOSAT. *Remote Sens. Environ.* **2022**, *280*, 113149. [CrossRef]
7. Li, B.; Li, J.; Liu, J.; Tang, S.; Chen, W.; Shi, P.; Liu, Y. Calibration experiments of CFOSAT wavelength in the Southern South China Sea by artificial neural networks. *Remote Sens.* **2022**, *14*, 773. [CrossRef]
8. Xu, Y.; Hauser, D.; Liu, J.; Jianyang, S.; Yan, C.; Chen, S.; Meng, J.; Fan, C.; Liu, M.; Chen, P. Statistical comparison of ocean wave directional spectra derived from SWIM/CFOSAT satellite observations and from buoy observations. *IEEE Trans. Geosci. Remote* **2022**, *60*, 5117520. [CrossRef]
9. Jiang, H.; Mironov, A.; Ren, L.; Babanin, A.; Wang, J.; Mu, L. Validation of wave spectral partitions from SWIM instrument on-board CFOSAT against in situ data. *IEEE Trans. Geosci. Remote* **2022**, *60*, 4204013. [CrossRef]
10. Hegermiller, C.A.; Antolinez, J.; Rueda, A.; Camus, P.; Perez, J.; Erikson, L.H.; Barnard, P.L.; Mendez, F.J. A multimodal wave spectrum-based approach for statistical downscaling of local wave climate. *J. Phys. Oceanogr.* **2017**, *47*, 375–386. [CrossRef]
11. Jiang, H.; Mu, L. Wave climate from spectra and its connections with local and remote wind climate. *J. Phys. Oceanogr.* **2019**, *49*, 543–559. [CrossRef]
12. Wyrtki, K. *Physical Oceanography of the Southeast Asian Waters: Scientific Results of Marine Investigations of the South China Sea and the Gulf of Thailand, NAGA Rep*; Scripps Institution of Oceanography: La Jolla, CA, USA, 1961; Volume 2, p. 195.
13. Sun, Z.; Zhang, H.; Liu, X.; Ding, J.; Cai, Z. Wave energy assessment of the Xisha Group Islands zone for the period 2010–2019. *Energy* **2021**, *220*, 119721. [CrossRef]
14. Su, H.; Wei, C.; Jiang, S.; Li, P.; Zhai, F. Revisiting the seasonal wave height variability in the South China Sea with merged satellite altimetry observations. *Acta Oceanol. Sin.* **2017**, *36*, 38–50. [CrossRef]
15. Jiang, H.; Babanin, A.V.; Liu, Q.; Stopa, J.E.; Chapron, B.; Chen, G. Can contemporary satellites estimate swell dissipation rate? *Remote Sens. Environ.* **2017**, *201*, 24–33. [CrossRef]
16. Jiang, H.; Chen, G. A Global View on the Swell and Wind Sea Climate by the Jason-1 Mission: A Revisit. *J. Atmos. Oceanic Technol.* **2013**, *30*, 1833–1841. [CrossRef]
17. Qian, C.; Jiang, H.; Wang, X.; Chen, G. Climatology of wind-seas and swells in the China Seas from wave hindcast. *J. Ocean Univ. China* **2020**, *19*, 90–100. [CrossRef]
18. Tolman, H. Treatment of unresolved islands and ice in wind wave models. *Ocean Model.* **2003**, *5*, 219–231. [CrossRef]
19. Mao, K.; Chen, X.; Wang, L. Research progress of spectral wave mode of archipelago or reef ocean region. *Acta Oceanol. Sin.* **2014**, *36*, 161–169. (In Chinese) [CrossRef]
20. Tang, S.; Chu, X.; Jia, Y.; Li, J.; Liu, Y.; Chen, Q.; Li, B.; Liu, J.; Chen, W. An appraisal of CFOSAT wave spectrometer products in the South China Sea. *Earth Space Sci.* **2022**, *9*, e2021EA002055. [CrossRef]
21. Xu, Y.; Liu, J.; Xie, L.; Sun, C.; Liu, J.; Li, J.; Xian, D. China-France Oceanography Satellite (CFOSAT) simultaneously observes the typhoon-induced wind and wave fields. *Acta Oceanol. Sin.* **2019**, *38*, 158–161. [CrossRef]

22. Wang, X.; Ichikawa, K. Coastal waveform retracking for Jason-2 altimeter data based on along-track echograms around the Tsushima Islands in Japan. *Remote Sens.* **2017**, *9*, 762. [CrossRef]
23. Liu, J.; Lin, W.; Dong, X.; Lang, S.; Yun, R.; Zhu, D.; Zhang, K.; Sun, C.; Mu, B.; Ma, J.; et al. First results from the rotating Fan Beam Scatterometer onboard CFOSAT. *IEEE Trans. Geosci. Remote* **2020**, *58*, 8793–8806. [CrossRef]
24. Li, X.; Xu, Y.; Liu, B.; Lin, W.; He, Y.; Liu, J. Validation and calibration of nadir SWH products from CFOSAT and HY-2B with satellites and in situ observations. *J. Geophys. Res. Oceans* **2021**, *126*, e2020JC016689. [CrossRef]
25. Hersbach, H.; Bell, B.; Berrisford, P.; Biavati, G.; Horányi, A.; Muñoz Sabater, J.; Nicolas, J.; Peubey, C.; Radu, R.; Rozum, I.; et al. ERA5 Hourly Data on Single Levels from 1959 to Present. Copernicus Climate Change Service (C3S) Climate Data Store (CDS). 2018. Available online: https://cds.climate.copernicus.eu/cdsapp#!/dataset/reanalysis-era5-single-levels?tab=overview (accessed on 2 February 2023).
26. Monaldo, F. Expected differences between buoy and radar altimeter estimates of wind speed and significant wave height and their implications on buoy-altimeter comparisons. *J. Geophys. Res. Oceans* **1988**, *93*, 2285–2302. [CrossRef]
27. Queffeulou, P. Long-term validation of wave height measurements from altimeters. *Mar. Geod.* **2004**, *27*, 495–510. [CrossRef]
28. Yaakob, O.; Hashim, F.E.; Mohd Omar, K.; Md Din, A.H.; Koh, K.K. Satellite-based wave data and wave energy resource assessment for South China Sea. *Renew. Energ.* **2016**, *88*, 359–371. [CrossRef]
29. Ye, H.; Li, J.; Li, B.; Liu, J.; Tang, D.; Chen, W.; Yang, H.; Zhou, F.; Zhang, R.; Wang, S.; et al. Evaluation of CFOSAT scatterometer wind data in global oceans. *Remote Sens.* **2021**, *13*, 1926. [CrossRef]
30. Yang, J.; Zhang, J. Validation of sentinel-3A/3B satellite altimetry wave heights with buoy and Jason-3 data. *Sensors* **2019**, *19*, 2914. [CrossRef]
31. Dobson, E.; Monaldo, F.; Goldhirsh, J.; Wilkerson, J. Validation of Geosat altimeter-derived wind speeds and significant wave heights using buoy data. *J. Geophys. Res. Oceans* **1987**, *92*, 10719–10731. [CrossRef]
32. Chen, G.; Lin, H. Technical note: Impacts of collocation window on the accuracy of altimeter/buoy wind-speed comparison-a simulation study. *Int. J. Remote Sens.* **2001**, *22*, 35–44. [CrossRef]
33. Shanas, P.R.; Kumar, V.S.; Hithin, N.K. Comparison of gridded multi-mission and along-track mono-mission satellite altimetry wave heights with in situ near-shore buoy data. *Ocean Eng.* **2014**, *83*, 24–35. [CrossRef]
34. Hanson, J.L.; Phillips, O.M. Automated analysis of ocean surface directional wave spectra. *J. Atmos. Oceanic Technol.* **2001**, *18*, 277–293. [CrossRef]
35. Ribal, A.; Young, I.R. 33 years of globally calibrated wave height and wind speed data based on altimeter observations. *Sci. Data* **2019**, *6*, 77. [CrossRef] [PubMed]
36. Dodet, G.; Piolle, J.-F.; Quilfen, Y.; Abdalla, S.; Accensi, M.; Ardhuin, F.; Ash, E.; Bidlot, J.; Gommenginger, C.; Marechal, G.; et al. The Sea State CCI dataset v1: Towards a sea state climate data record based on satellite observations. *Earth Syst. Sci. Data* **2020**, *12*, 1929–1951. [CrossRef]
37. Jiang, H.; Fu, G.; Ren, L. Evaluation of coastal altimeter wave height observations using dynamic collocation. *IEEE Trans. Geosci. Remote* **2022**, *60*, 1–8. [CrossRef]
38. Nencioli, F.; Quartly, G. Evaluation of Sentinel-3A wave height observations near the coast of southwest England. *Remote Sens.* **2019**, *11*, 2998. [CrossRef]
39. Gomez-Enri, J.; Vignudelli, S.; Quartly, G.; Gommenginger, C.; Cipollini, P.; Challenor, P.; Benveniste, J. Modeling Envisat RA-2 waveforms in the coastal zone: Case study of calm water contamination. *IEEE Geosci. Remote S.* **2010**, *7*, 474–478. [CrossRef]
40. Liang, G.; Yang, J.; Wang, J. Accuracy evaluation of CFOSAT SWIM L2 products based on NDBC buoy and Jason-3 altimeter data. *Remote Sens.* **2021**, *13*, 887. [CrossRef]
41. Roblou, L.; Lamouroux, J.; Bouffard, J.; Lyard, F.; Le Hénaff, M.; Lombard, A.; Marsaleix, P.; De Mey, P.; Birol, F. Post-Processing Altimeter Data towards Coastal Applications and Integration into Coastal Models. In *Coastal Altimetry*; Vignudelli, S., Kostianoy, A.G., Cipollini, P., Benveniste, J., Eds.; Springer: Berlin/Heidelberg, Germany, 2011; pp. 217–246. [CrossRef]
42. Andersen, O.B.; Knudsen, P. The role of satellite altimetry in gravity field modelling in coastal areas. *Phys. Chem. Earth Part A Solid Earth Geod.* **2000**, *25*, 17–24. [CrossRef]
43. Labroue, S.; Gaspar, P.; Dorandeu, J.; Zanifé, O.Z.; Mertz, F.; Vincent, P.; Choquet, D. Nonparametric Estimates of the Sea State Bias for the Jason-1 Radar Altimeter. *Mar. Geod.* **2004**, *27*, 453–481. [CrossRef]

Disclaimer/Publisher's Note: The statements, opinions and data contained in all publications are solely those of the individual author(s) and contributor(s) and not of MDPI and/or the editor(s). MDPI and/or the editor(s) disclaim responsibility for any injury to people or property resulting from any ideas, methods, instructions or products referred to in the content.